

A comparison of the limited-area 3DVAR and ETKF-En3DVAR data assimilation using radar observations at convective-scale for the Prediction of Typhoon Saomai (2006)

Feifei Shen^{1,2*} Ming Xue^{1,2} and Jinzhong Min¹

¹ Key Laboratory of Meteorological Disaster, Ministry of Education (KLME) /Joint International Research Laboratory of Climate and Environment Change (ILCEC) /Collaborative Innovation Center on Forecast and Evaluation of Meteorological Disasters (CIC-FEMD), Nanjing University of Information Science & Technology, Nanjing 210044, China

²Center for Analysis and Prediction of Storms and School of Meteorology, University of Oklahoma, Norman, Oklahoma 73072, USA

Accepted by Meteorological Applications

February, 2017

*Corresponding author address:

Feifei Shen

Nanjing University of Information Science & Technology
ffshen.nuist@gmail.com

Abstract

The ensemble transform Kalman filter based-Ensemble/3DVAR (ETKF-En3DVAR) data assimilation (DA) systems are employed to evaluate the potential value of assimilating radar radial wind (V_r) data for the analysis and forecast of typhoon Saomai (2006). The DA system conducts cycling assimilation every 30 minutes when Saomai started to enter the radar coverage. Within the DA cycles, the control analysis is updated by the ETKF-En3DVAR algorithm whereas the forecast ensemble perturbations in the hybrid scheme are updated by the ETKF algorithm. The benefits from the use of the flow-dependent ensemble covariance are explored by comparing the analysis increments, analysis, and subsequent forecasts from the hybrid scheme with those by a pure 3DVAR using static background error covariance. Sensitivity to the horizontal correlation scale in the 3DVAR and the vertical covariance localization in the hybrid are also explored.

The reduced horizontal correlation scale in the 3DVAR yields much more reasonable circulation analyses than the default scale. The vertical covariance localization scale specified in terms of geometric height instead of model levels allows for desirable spreading of V_r data to the surface. It seems that the assimilation with the hybrid method lead to further improved vortex intensity forecast and track forecast of the typhoon compared to those in the analyses from the global forecast system (GFS) and 3DVAR. Results also indicated that the hybrid has significant effect on the 12-hour accumulated rainfall forecasts. Such improvements for analysis and forecast are probably due to the utilization of the flow-dependent background error covariance.

Keywords: WRF model; hybrid assimilation; radar radial velocity

1. Introduction

China suffers more typhoon damage than most other countries, and there are approximately nine tropical cyclones (TCs) landing in China coast each year in average (CMA; Yu, 2007; Song et al., 2010; Li et al., 2012). Accurate prediction of landfalling TCs in terms of the track and intensity is therefore crucial to protect the life and property in coastal areas. Improvements to TC forecasting can be attributed mainly to the improvements of numerical weather prediction (NWP) models, but also to more effective data assimilation (DA) approaches that can optimize based on both the forecast background and observations (Li et al., 2015; Wang et al., 2016). The uncertainties in DA procedures are typically characterized by error covariance matrices of the background state and observations. The background error matrices play important roles in determining the level of impacts of observations and how the observation information is distributed spatially and among the analysis variables. Given the localized characteristics of strong TC vortices and the associated large wind, temperature and moisture gradients, and fast forecast error growth with typical TC systems, it is difficult for DA systems to obtain accurate analysis of the inner core structures that are dynamical and thermodynamical consistent using static background error covariance (BEC) typically employed in 3D variational (3DVAR) DA

systems that are in common use at operational NWP centers. Even with a 4D variational (4DVAR) DA system, the use of flow-dependent BEC will still be beneficial.

Recently, ensemble-based DA techniques (Evensen, 1994) have been explored to yield better initial conditions (ICs) for TC forecasts and in some cases for initializing ensemble forecasts also (Zhang et al., 2009; Torn, 2010; Wu et al., 2010; Dong and Xue, 2013; Wang et al., 2014; Zhu et al., 2016). All these studies suggest that short-term ensemble forecasts can provide estimates of flow-dependent BEC and improve the subsequent forecasts. With ensemble sizes of 30 to 100 that are typically used in ensemble DA systems, the covariance matrix is rank deficient and result in sampling errors.

One potential solution to this problem is to combine the traditional static BEC with ensemble-derived BEC, as firstly proposed by Hamill and Snyder (2000), forming the so-called ensemble-variational (EnVar) hybrid method. Lorenc (2003) realized the combination of the BECs by extending the control variables (ECV) in the 3DVAR cost function. Among the hybrid DA studies, better analysis and forecast of TC track initialized with hybrid DA approach than 3DVAR methods are found in both global (Buehner et al. (2010a,b) and regional (Wang, 2011; Poterjoy and Zhang, 2014; Shen and Min, 2015; Ito et al., 2016; Wang et al., 2017) models. In Wang (2011), an ensemble transform Kalman filter (ETKF; Bishop et al., 2001) method was employed to update the forecast ensemble in the hybrid scheme. Shen and Min (2015) applied an ensemble of data assimilation technique based on perturbation of observations (EDA, Houtekamer et al., 1996) to updated the ensemble members with a different set of randomly perturbed observations. These studies focused on TC track forecasting at a relatively coarse resolution, without assimilating radar observations. Particularly, EDA method is relatively expensive due to its necessity of analysis for each ensemble member.

Recent studies (Li et al., 2012; Shen et al., 2016) have assimilated radial velocity (V_r) observations using the hybrid method to initialize the TCs forecasts with their focus on the Atlantic basin. As is known to all, TCs are also frequent in the western North Pacific (WNP) causing severe damage along China's coast. According to the author's best knowledge, the utility of the ensemble transform Kalman filter based-Ensemble/3DVAR (ETKF-En3DVAR) approach that assimilates V_r observations at cloud-scale resolution to the analysis and forecasts of landfalling TCs over WNP has not been examined in the previously published studies. This study serves this purpose.

In our current study, the emphasis is put on the impacts of V_r data covering the inner core precipitation regions within a TC, on both track and intensity forecasts using a 5 km convection-permitting grid spacing. The test case to be investigated is Saomai (2006), one of the strongest landfalling TCs ever recorded in China (Zhao et al., 2008). The V_r data from Wenzhou radar (WZRD) are assimilated to examine its impact on the track forecasting and intensity. Recent research by Zhao et al. (2012) explored the impacts of assimilating of Ground-based velocity track display method (GBVTD) retrieved winds from one radar for the same super typhoon Saomai during its landfall, and found that the assimilation of retrieved winds can yield

better forecasts compared to those initialized by assimilating Vr data directly. Their results suggest that the improvements obtained by the GBVTD method are primarily due to the better spatial coverage of the typhoon inner core region from the retrieved winds compared to Vr data. It should be noted that the limitations of the GBVTD method is that the retrieved winds do not contain asymmetric wind components for wavenumbers beyond 3. In addition, the most important way of our work differs from Zhao et al (2012) is that we using the ETKF-En3DVAR method which adopted the flow-dependent BEC whereas they employing an Advanced Regional Prediction System (ARPS) 3DVAR DA technique.

Section 2 introduces the ETKF-En3DVAR technique. Section 3 presents the radar data and the experimental settings. Section 4 discusses the experiment results. Conclusions and discussions are given in section 5.

2. The ETKF-En3DVAR algorithms

The cost function of the ETKF-En3DVAR is defined as

$$\begin{aligned} J(\mathbf{x}_1, \mathbf{a}) &= \beta_1 J_1 + \beta_2 J_e + J_o \\ &= \beta_1 \frac{1}{2} (\mathbf{x}_1)^T \mathbf{B}^{-1} (\mathbf{x}_1) + \beta_2 \frac{1}{2} (\mathbf{a})^T \mathbf{A}^{-1} (\mathbf{a}) + \frac{1}{2} (\mathbf{y}^o - \mathbf{H}\mathbf{x})^T \mathbf{R}^{-1} (\mathbf{y}^o - \mathbf{H}\mathbf{x}). \end{aligned} \quad (1)$$

J_1 is the background term associated with the static \mathbf{B} , J_e is the term related to the ensemble covariance, \mathbf{a} is the ECV. \mathbf{A} controls the spatial correlation of \mathbf{a} . J_o is the observation term. $\mathbf{y}^o = \mathbf{y}^d - H(\mathbf{x}^b)$ is the innovation vector as in 3DVAR; \mathbf{y}^d denotes the observation; \mathbf{x}^b is the background forecast, and \mathbf{H} is the linearized observation operator. Two coefficients, b_1 and b_2 , determine how much weight is prescribed to the ensemble BEC and the static BEC, which are constrained such that

$$\frac{1}{b_1} + \frac{1}{b_2} = 1. \quad (2)$$

The horizontal localization is performed using recursive filters (Hayden and Purser, 1995). Empirical orthogonal functions (EOFs) are employed for the vertical localization by transforming the ECV \mathbf{a} in Eq. (1). A general formulation to form the vertical covariance matrix, from which the EOFs are derived, can be written as,

$$\text{Cov}(k_1, k_2) = \exp\left(-\frac{d^2}{L^2}\right), \quad (3)$$

where $\text{Cov}(k_1, k_2)$ represents the correlation between model levels k_1 and k_2 , L is the vertical

localization radius, and d stands for the distance between k_1 and k_2 . Similarly, the default vertical covariance matrix used in WRF model data assimilation system (WRFDA) is defined as

$$\text{Cov}(k_1, k_2) = \exp\left(-\frac{d^2}{\left(10\frac{k_1}{N}\right)^2}\right), \quad (4)$$

Where N is the total number of model levels. The localization radius $10\frac{k_1}{N}$ is in proportion to the model height, which means the localization radius is shorter when model level is lower. For V_r observations, more advanced correlation methods may be necessary to better spread the observation information to vertically stretched grid, which will be explicated in section 4a.

3. Numerical experiments

3.1. WRF model and radar data processing

A version 3.5 of the WRF model (Skamarock et al., 2005) is employed to conduct numerical experiments. All experiments are performed over a single domain shown in Figure 1 that has a 401×401 horizontal grid points spaced 5 km apart and covers the TC core area with 41 vertical levels and a model top of 100 hPa. The model physics include the WRF Single-Moment 6-Class scheme (Hong et al., 2004); the Rapid Radiative Transfer Model for longwave radiation with six molecular species (Mlawer et al., 1997); the MM5 shortwave radiation scheme (Dudhia, 1989); the Yonsei University (YSU) planetary boundary layer scheme (Noh et al., 2003); and the Kain-Fritsch cumulus parametrization (Kain, 2004). In the current study, the Level-II V_r observations assimilated were from the WZRD located in the east coast of China. During the landfall of typhoon Saomai, the WZRD is operated in volume coverage pattern 21 (VCP21) scanning strategy containing nine elevation angles from 0.5° to 19.5° . The quality control of the V_r observations is conducted using the 88d2arps package in the ARPS model and the SOLO software (Oye et al., 1995) developed by NCAR to identify unwanted radar echoes. The observational error for V_r data are empirically set as 2 m s^{-1} in the current study.

3.2. The data assimilation experiments setup

Before the real case experiments are carried out, we conduct single observation tests to investigate the impact of conducting vertical covariance localizations. For the real case of Saomai, a total of five experiments were performed to examine the impact of assimilating V_r data with different DA method. Table 1 summarizes the experiments. The simulation without any V_r observation DA (NoDA) is performed with initial and lateral boundary conditions (LBCs) derived from the NCEP operational GFS analysis at 0000 UTC 10 August 2006. Additionally, two groups of DA experiments were conducted in our current study. The first group of the DA experiments denoted as 3DVARa and 3DVARb which assimilated the V_r observations using the WRF 3DVAR method. The DA experiments conducted in the second group are denoted as HybridF and HybridH respectively.

A schematic diagram is provided by Figure 2 to depict the assimilation and forecast step for all experiments. In all DA experiments, the assimilation period is from 0300UTC to 0600 UTC August at half hour intervals. The two 3DVAR experiments contain three steps: (1) a 3 h forecast initialized from the GFS analysis at 0000 UTC 10 August; (2) assimilation of Vr data every 30 minutes until 0600 UTC 10 August; and (3) a 12 h deterministic forecast initialized by the final analysis cycle in step (2) at 0600 UTC 10 August.

For the second group of the hybrid DA experiments, similar steps are conducted: 1) 3 h ensemble forecasts initialized from perturbed GFS analysis valid at 0000 UTC 10 August are conducted to calculate the flow-dependent ensemble BEC. The LBCs and the ICs of the ensemble forecasts are randomly sampled from the GFS analyses based on the static BEC; 2) same to the 3DVAR DA experiments just instead of using the hybrid method; 3) The hybrid analysis at the end of DA cycles is employed to initialize a 12 h deterministic forecast.

As mentioned by many other studies (Li et al., 2015; Shen and Min, 2015), the covariance matrix derived using the National Meteorological Center (NMC) method (Parrish and Derber, 1992) with option 5 (CV5; Barker et al., 2012) based on the forecasts with different leading time mainly reflects the large-scale correlations. Following Li et al. (2012) and Shen and Min (2015), we rescale the static BEC by reducing the spatial correlation scale to 10% in 3DVARb, and in HybridH, while 3DVARa uses the default correlation scale for a comparison purpose. In HybridF and HybridH, two different sets of BEC weighting factors ($1/\beta_2 = 1/1.001$ and $1/2$) were adopted. The former applies a 100% ensemble covariance, and the latter corresponds to a blend of 50% static BEC and 50% ensemble BEC. In HybridF, although 0% static BEC is used, the experiment is still conducted in the traditional EnVar framework. HybridF is different from the traditional EnKF. The analysis of HybridF is conducted by extending the control variables in the cost function in Eq. (1) with all observations assimilated simultaneously, while the analysis is achieved by solving the Kalman gain with observations assimilated sequentially.

4. Results and discussion

In this section, the analyses and forecasts of the 3DVAR and hybrid experiments are evaluated. Diagnostics are conducted to understand how Vr data from WZRD improve the analysis of TC and to examine how the improvement in the analyses impact the subsequent forecasts. Sensitivity to the horizontal correlation scale of the BEC is examined by comparing the results of 3DVARa and 3DVARb first, before examining the hybrid DA experiments. As in Li et al. (2012), before we assimilate the full set of Vr observations, we first examine the increments produced by a single Vr observation, which can help us understand the behaviors of the hybrid DA method with different configurations.

4.1 Single observation experiments

Single observation tests with different vertical covariance localization methods are performed to estimate the spread of Vr observation by the ensemble BEC. Three initial

experiments were conducted. Experiment Vertloc_d used the default vertical covariance localization method developed by WRFDA described in section 2. The second experiment used the vertical localization method based on the geometric height (unit in km) rather than model levels, which is denoted as Vertloc_km. The third experiment, without any vertical covariance localization method (referred to as Vertloc_no), serves as a baseline for evaluating the vertical covariance localization in the hybrid scheme. The impact of assimilating a single Vr observation at 3306.7 m above sea level with a -48.56 m s^{-1} innovation (observation minus background) is examined for all experiments at 0300 UTC 10 August 2006. The background is interpolated from the GFS final analysis at 0300 UTC 10 August 2006. The resulting analysis increments of the wind speed by HybridF from various DA experiments are illustrated in Figure 3. In both hybrid experiments, HybridF and HybridH, the radiuses for the vertical localization and horizontal localization are 3 and 20 km respectively, which are empirically determined. Sensitivity tests with different horizontal localization radiuses as 20, 60, 100, 600, and 1000 km are also conducted, among which the 20 km test yields the most reasonable increment (not shown). In Figure 3a, noisy wind increments are found at the upper levels, reaching the model top without vertical localization. As expected, the other two experiments with different vertical covariance localization methods avoid spurious correlation in a good way. For the Vertloc_km experiment, the analysis increment is efficiently confined close to the observation location, indicating that the new implemented vertical localization scheme is efficiently useful for Vr DA. A similar situation is shown in the Vertloc_d experiment, but the impact of Vr data could not spread to the surface.

4.2 Results of Saomai case

4.2.1 Wind increments

The horizontal wind increments from 3DVARa, 3DVARb, HybridF, and HybridH at 700 hPa, at 0300 UTC 10 August 2006 in the first analysis cycle are compared to show the impact of the Vr DA in Figure 4. Cyclonic and anti-cyclonic horizontal increment patterns in 3DVARa are observed of rather large scales in Figure 4a. The cyclonic and anti-cyclonic patterns are found to the southeast and the northwest of the observed TC center, respectively. At the typhoon center location, northeasterly wind increment is observed. Previous studies (e.g., Xiao and Sun, 2007; Li et al., 2012) also found such similar wind increments when assimilating Vr data with WRF 3DVAR. There are no clear vortical wind increments in the analysis in the event that the background significantly underestimates the vortex intensity with the default BEC using the NMC method. The static BEC causes inappropriate large amount of smoothing of the Vr data and inappropriate large spreading of Vr observation information outside the region of the data coverage. As Sugimoto et al. (2009) pointed out that the BECs generated by the NMC method appears to be overestimated in terms of the spatial correlations scales. Therefore, the horizontal spatial scales in the BECs for assimilations of the Vr data with high spatial resolution should be tuned much smaller, which is quite regular practice in the ARPS with 3DVAR method (e.g., Hu et al., 2006; Schenkman et al., 2011). 3DVARb reduces the horizontal spatial correlation scale by a tuning factor of 0.1. Figure 4b shows that with the tuned horizontal spatial correlation scale a

strong cyclonic circulation increment is observed at 700 hPa around the observed center of TC, indicating an enhancement to the weak background vortex. Additionally, the large wind increments are more reasonably confined to the region of the observed TC center. However, it should be noted that even we rescale horizontal spatial correlation scale, noticeable anticyclonic incremental circulation is still found in northeast of the observation TC center. Recent studies by Xie and MacDonald (2012) and Sun and Wang (2013) suggested that the use of stream function and velocity potential as momentum control variables might not be suitable for analysis over a regional domain for small-scale problems. Other DA systems that using Vr data which adopt the Cartesian wind components (u,v) as momentum control variables. For example, Zhao et al. (2012) assimilated the Vr data for the same case of typhoon Saomai within the ARPS 3DVAR system which adopt the Cartesian wind components (u,v) as momentum control variables, no anticyclonic analysis increments were found. In the future, we need to do more research on this issue. Nevertheless, a thorough research on this issue is beyond the scope of our current study. The HybridF analysis after the first DA cycle yielded a clear asymmetric cyclonic pattern around the observed TC center (Figure 4c). With the use of the full weight ensemble BEC, the pattern of the wind increment is less axisymmetric, which can be attributed to the spatially inhomogeneous ensemble BEC estimated from the ensembles. HybridH placed a 50% weighting for both the static and ensemble BEC; the pattern of the wind increments is rather close to that of 3DVARb. However, the magnitude of the wind increments is in between those of 3DVARb and HybridF (Figure 4d).

4.2.2 Diagnostics during the DA cycles

To examine how the model state fit the observations, the root-mean-square error (RMSE) of the background forecasts and the analyses against the Vr observations of 3DVARb, HybridH, and HybridF are presented in Figure 5a. For the hybrid DA experiments, the ensemble mean is utilized to calculate the innovation. The RMSE of Vr reduced gradually during the analysis cycles in all DA experiments. Also note that the RMSE of Vr reduced significantly after the first DA cycle, which is mainly due to the largest observation increments obtained in all DA experiments. In the following DA cycles, the RMSE of the analyses range between 3.5 and 4.5 m s⁻¹. Such magnitudes of the errors are close to the observational errors applied in the Vr DA. The short term forecasts during cycles initialized from the analyses generally cause the Vr RMSE increasing by roughly 3 m s⁻¹. Generally, HybridF yields the least analysis error, while 3DVARb the largest error and HybridH is in-between. Similar results are also found for the 30-min forecasts. At the end, the RMSE of HybridF and HybridH are about 3.5 m s⁻¹, while the RMSE of 3DVARb is about 4.5 m s⁻¹. Overall, the RMSE of all DA experiments, especially for the hybrid DA experiments, are largely reduced compared to the initial RMSEs of about 14 m s⁻¹.

The minimum sea level pressure (MSLP) from the background forecasts and the analyses during the DA cycles are plotted in Figure 5b to investigate the DA impact on the analyzed typhoon intensity from 3DVARb, HybridH, and HybridF. The best track data from CMA are also plotted for verification. The MSLP stay overall constant as 920 hPa during the 3 h period.

The analyzed MSLP decreases by more than 20 hPa during the first analysis cycle in HybridF and HybridH (Figure 5b), while for the rest analysis cycles, the MSLP from analyses decrease slightly. The reduction of MSLP through the forecast is due to the pressure adjustments to the analyzed winds by DA. For the rest of the DA cycles, the center pressure of HybridF and HybridH are relatively stable at roughly 950 hPa. It seems that MSLP decreased more quickly in the short term forecasts during DA analyses in the hybrid DA experiments than it did in 3DVARb experiment. At the end of the DA, the MSLP in the final analysis from HybridF is about 9.0 hPa lower than that in HybridH, yielding the least MSLP error.

4.2.3 The analyzed typhoon structures

The MSLP along with the maximum surface wind (MSW) from NoDA, 3DVARb, HybridF, and HybridH at 0600 UTC are presented in Figure 6. Obviously, the typhoon intensity in the GFS analysis is too weak (Figure 6a). The MSW in the best track data is close to 60 m s^{-1} while the MSW in NoDA is only around 14.7 m s^{-1} . After DA, 3DVARb, HybridH, and HybridF yield MSLP (MSW) as 953 hPa (47.4 m s^{-1}), 946 hPa (49.1 m s^{-1}), and 937 hPa (50.0 m s^{-1}), respectively. The improvements of the typhoon intensity can be attributed to the flow-dependent BEC, since the multivariate correlation between the surface pressure and the wind is stronger than that in the static BEC. Besides the improvement in terms of the intensity, the location of analyzed typhoon is closer to the observed center with radar DA (Figure 6). In addition, it was also found that the center locations from HybridF were more accurate than both 3DVARb and HybridH.

Figure 7 shows the east-west vertical cross-sections through the analyzed typhoon center for the horizontal wind speed and potential temperature for NoDA, 3DVARb, HybridF, and HybridH. The weak vortex with a broad eye is evident without obvious inner core structure (Figure 7a). The GFS analysis as the background is not able to resolve any inner-core structure with a coarse resolution. The typhoon structure in 3DVARb and HybridH (Figure 7b, d) are well improved, with a stronger circulation compared to that in NoDA. HybridF (Figure 7c) yields a more upright and asymmetric eyewall than 3DVARb does. The potential temperature contours of HybridF and HybridH bend downward below $\sim 600 \text{ hPa}$, indicating a warmer core structure (Figure 7c,d) as opposed to those in 3DVARb (Figure 7b).

To further examine the structures of analyzed TC, the azimuthally average tangential wind and temperature anomaly at 0600 UTC are shown in Figure 8. The temperature anomaly is defined as the deviation from the temperature averaged over a horizontal area within a radius of 180 km centered at the TC center (Liu et al., 1999). The azimuthally averaged horizontal winds from the DA experiments are substantially stronger compared to those in NoDA, among which HybridF yields the strongest wind. In HybridF, the horizontal winds show much larger horizontal gradients in the inner core area compared to the other three experiments. The typhoon circulation directory from GFS analysis in NoDA is very weak with a broad eye (Figure 8a). Consistent with a stronger circulation in HybridF, a warm core is most obvious in its eye region at about 6 km, which is also consistent with observed common TC structures (Hawkins and Imbombo, 1976;

Liu et al., 1999; Emanuel, 2005; Halverson et al., 2006). In Figure 8b, the radius of maximum wind in the vortex reaches roughly 20 km. Similar results were found in HybridF and HybridH. For HybridF, the structures of the temperature anomalies and the horizontal winds are close to those of HybridH except with about 5 m s^{-1} stronger winds around the surface region (Figs. 8c and 8d). Generally speaking, the three DA experiments significantly improved the vortex circulation as well as the warm core structure. The Saomai analyzed by HybridF was more realistic than 3DVARb and HybridH.

4.2.4 Track and intensity prediction

In this subsection, the forecast skills of the typhoon track and intensity from all experiments are discussed. Figure 9a shows the 12 h track forecasts along with the best tracks from CMA, while the corresponding track errors, MSLP, and MSW at different forecast lead time are shown in Figure 9 b, c, d. The track errors at 0600 UTC are smaller than 20 km from all DA experiments initially. In NoDA, the predicted typhoon tracks have a southward bias (Figure 9a), resulting in the largest track errors: they exceed 65 km at the end of forecast, with a 12 h mean track error of about 43 km (Figure 9b). Particularly worth mentioning is that the predicted typhoon tracks of NoDA have a northwestward bias in Figure 9a of Zhao et al. (2012). The differences in the results of NoDA experiments are caused by the ICs and LBCs. Zhao et al., (2012) use Japan Meteorological Agency 6 hourly gridded regional analysis to create the ICs and LBCs for the ARPS model whereas we used NCEP operational GFS analysis data as the ICs and LBCs for the WRF model. In comparison, the 12 h mean track errors in 3DVARb, HybridH, and HybridF are reduced to 30 km, 13 km, and 10 km, respectively (Figure 9b). In the first three hours of the forecast before the typhoon's landfall, the tracks of the DA experiments are comparable with a small track error less than 20 km; the predicted track of HybridF fit the best track most closely, probably due to its improved initial vortex location and structure indicated in Figure 6. Also note that after the 9-h forecast, the vortex of 3DVARb tended to move northwest too fast, resulting in the track errors increasing with forecast lead time to over 46 km. However, the predicted tracks of the two hybrid DA experiments are close to each other. HybridF has the least track error during most of the forecast period. The main effects on the track are presumably due to the changes of the intensity, structure, and location of the analyzed typhoon.

The typhoon Saomai's MSLP and MSW during the 12 h forecasting leading time are presented in Figure 9c, d. The observed typhoon starts at 920 hPa for MSLP. Obviously, NoDA underestimated the strong vortex for the most of the forecasting period with highest MSLP. It is obvious that the radar DA is able to improve the intensity forecasts. Also note that the pressures in HybridF and HybridH rise at similar rates to the best track data before 1200 UTC. Their rates of rise are lower than the best track from 1200 UTC to 1500 UTC, which might be caused by the errors in the forecast model. In comparison with NoDA, 3DVARb, and HybridH, HybridF preponderant in terms of forecasting the MSLP. In Figure 9d, the MSW speeds for 3DVARb, HybridH, and HybridF are notably higher during the 12 h forecast period compared to those in

NoDA, but slightly weaker compared to the best track data. The MSW of HybridH and HybridF are comparable.

4.2.5 Precipitation forecasting

The total accumulated precipitations during the 12 h forecast period from the four experiments are plotted in Figure 10 along with the automatic weather station rainfall observations. The NoDA experiment forecasts the precipitation pattern and amount rather poorly. It significantly underestimates the accumulated precipitation over land. Also note that there is a southward bias in the precipitation location, which may be due to its southward track bias and low intensity. According to the rainfall observation data, there is a maximum precipitation near 27.5°N, close to the radar center and a band of heavy precipitation along the coast of Zhejiang and Fujian Province. HybridF showed significant improvement in forecasting the convective spiral rain band near its inner core area. 3DVARb yields too much spurious precipitation in the north of the vortex in southern Zhejiang Province. The heavy rain band in the north of the provincial border and other precipitation maximums in the south of the border are both well captured by HybridF and HybridH, although the strength and coverage are underpredicted (Figure 10c, d). Assimilating Vr data in HybridF enhanced the precipitation forecast in northern Fujian Province better than that in HybridH (Figure 10c, d). In terms of the weaker precipitation, all experiments produced similar general pattern to the available observations. In general, HybridF yielded the best distribution and magnitude for the precipitation probably due to its improved track, intensity and structure forecast of the typhoon.

To further evaluate the precipitation forecast skill, equitable threat scores (ETS, also called Gilbert skill score; Schaefer, 1990) and bias scores based on the 12 h accumulated precipitation forecasts are plotted in Figure 11 for several prescribed precipitation thresholds. It is found that the ETS scores from the three Vr DA experiments are much higher than that from NoDA. Specifically, for most thresholds, HybridF obtains the highest ETS scores with least bias (close to one) and yields slightly higher ETS scores than HybridH as well. The NoDA experiment without Vr DA overpredicts the weak precipitation and underpredicts the heavy precipitation, especially for precipitation above 110 mm, which is related to a weaker predicted typhoon. The ETS scores from the NoDA experiment drop quickly above 50 mm threshold. For all thresholds, the hybrid DA experiments obtained higher ETSs compared to 3DVARb, with its improvements over 3DVARb more obvious when the precipitation threshold increases.

5. Conclusions

This study investigated the impact of assimilating Vr data using the ETKF-En3DVAR versus the traditional variational DA methods on the analysis and forecast of typhoon Saomai (2006). With such a system, the flow-dependent BEC estimated from the ensemble forecasts is used in the variational framework, and the ensemble mean is updated by using a hybridized static BEC and ensemble BEC while the ensemble perturbations are updated with the computationally efficient ETKF. Vertical localization schemes are also preliminarily explored in our hybrid

framework, which are based on the geometric height rather than model levels. The following are the main conclusions from these experiments by comparing the analyses and subsequent forecasts:

(1) The default BEC estimated with the NMC method only reflects synoptic scale error structures and always ignores strong vortex in the background. With the tuned horizontal spatial correlation scale in 3DVARb, appropriate adjustment to the weak background vortex is observed compared to that without tuning.

(2) Experiments with different vertical covariance localization methods avoid spurious correlations in a good way. The vertical localization scheme based on a 3 km length scale is useful for Vr assimilation, resulting in analysis increments more efficiently confined around the location of the observation, which could reach the surface.

(3) On average, the analyses of the three DA experiments (3DVARb, HybridH, and HybridF) fit the Vr data well. The root-mean-square errors of Vr yield the largest reduction in the first analysis cycle in three experiments. In general, HybridF produces the least analysis error, while 3DVARb the largest error and HybridH is in-between. Similar results are found for the 30-min forecasts.

(4) For the DA cycles, the MSLP of HybridF and HybridH are well maintained at around 950 hPa. In particular, it is found that MSLP in the hybrid experiments decreases much more quickly during the short term forecasts between different analyses than it did in 3DVARb. At the end of DA cycles, the final analysis of HybridF yields the least MSLP error.

(5) For the analyzed typhoon structures, the center location from HybridF is more accurate than both 3DVARb and HybridH. Generally, three DA experiments are able to improve the vortex circulation and the thermodynamical core structure. HybridF yields much stronger vortex favorably in terms of the circulation and eyewall compared to other DA experiments.

(6) The track forecast with the hybrid DA method is significantly superior to the 3DVAR method. The tracks of the two hybrid DA experiments are very close. In comparison with NoDA, 3DVARb, and HybridH, HybridF preponderant in terms of forecasting the MSLP. The MSW speeds for 3DVARb, HybridH, and HybridF are notably higher during the 12h forecast period compared to that in NoDA, but slightly weaker compared to the observed track. The MSW of HybridH and HybridF are comparable to each other.

(7) The ETS scores from the three Vr DA experiments are much higher than that from NoDA. For most thresholds, HybridF obtains the highest ETS scores with least bias (close to one) and yields slightly higher ETS scores than HybridH as well. The NoDA experiment without radar DA overpredicts the weak precipitation and underpredicts the heavy precipitation. For all thresholds, the hybrid experiments gain higher ETSs compared to 3DVARb, with its improvements over 3DVARb more significantly when the precipitation threshold increases.

These findings suggest that hybrid DA method can improve the analysis and forecasts compared to 3DVAR method. There are some issues for further exploration and improvements. In our current study, ETKF-En3DVAR is employed to assimilate the Vr data to initialize the TC

forecast. Direct and thorough comparisons of WRF ETKF-En3DVAR system with other hybrid DA methods such as EDA-En3DVAR are under way so as to reveal the impacts of different ensemble generation techniques within the EnVar framework for the analysis and forecasting of TCs at the convective scale. It should also be pointed out that no vortex relocation approach (Hsiao et al., 2010; Gao et al., 2014) is applied and only Vr data are used. Further work will examine the impact of conducting vortex relocation scheme and assimilating more in-situ observations within the ETKF-En3DVAR. It is acknowledged that the above findings and conclusions are based on a single super typhoon case. Further studies with more TC cases in terms of assimilating more complete observations types are required to obtain more comprehensive results. In addition, we plan to develop and establish the four-dimensional ensemble-variational (4DEnVar) technique based on the WRFDA system for TC forecasts as a natural extension of the current study.

Acknowledgements This research was primarily supported by the 973 Program (Grant No. 2013CB430102), the Natural Science Foundation of Jiangsu Province under Grant No. BK20160954, the Beijing Funding from Jiangsu Research Institute of Meteorological Science (Grant No. BJG201510, BJG201604), and the Priority Academic Program Development of Jiangsu Higher Education Institutions (PAPD). We appreciate the comments and suggestions provided by LaDue, Daphne S. that significantly improved the content and clarity of this manuscript. The first author also acknowledges Shizhang Wang, Kefeng Zhu, and Yongzuo Li for helpful discussions and assistance with the initial drafts. Supercomputers at TACC, University of Texas, and SGI Altix3700 BX2, Nanjing University of Information Science & Technology were used.

References

- Barker, D., and Coauthors, 2012: The Weather Research and Forecasting Model's Community Variational/Ensemble Data Assimilation System: WRFDA. *B Am Meteorol Soc*, 93, 831-843.
- Bishop, C. H., B. J. Etherton, and S. J. Majumdar, 2001: Adaptive sampling with the ensemble transform Kalman filter. Part I: Theoretical aspects. *Mon. Wea. Rev.*, 129, 420.
- Buehner, M., P. L. Houtekamer, C. Charette, H. L. Mitchell, and B. He, 2010a: Intercomparison of variational data assimilation and the ensemble Kalman filter for global deterministic NWP. Part I: Description and single-observation experiments. *Mon. Wea. Rev.*, 138, 1550-1566.
- Buehner, M., P. L. Houtekamer, C. Charette, H. L. Mitchell, and B. He, 2010b: Intercomparison of variational data assimilation and the ensemble Kalman filter for global deterministic NWP. Part II: One-month experiments with real observations. *Mon. Wea. Rev.*, 138, 1567-1586.
- Dong, J. L., and M. Xue, 2013: Assimilation of radial velocity and reflectivity data from coastal WSR-88D radars using an ensemble Kalman filter for the analysis and forecast of landfalling hurricane Ike (2008). *Quarterly Journal of the Royal Meteorological Society*, 139, 467-487.

- Dudhia, J., 1989: Numerical study of convection observed during the winter monsoon experiment using a mesoscale, two-dimensional model. *J. Atmos. Sci.*, 46, 3077-3107.
- Emanuel, K. A., 2005: *Divine wind : the history and science of hurricanes*. ed. Oxford University Press, x, 304 p.pp.
- Evensen, G., 1994: Sequential data assimilation with a nonlinear quasi-geostrophic model using Monte Carlo methods to forecast error statistics. *J. Geophys. Res.*, 99, 10143-10162.
- Gao, F., P. P. Childs, X. Y. Huang, N. A. Jacobs, and J. Z. Min, 2014: A relocation-based initialization scheme to improve track-forecasting of tropical cyclones. *Adv Atmos Sci*, 31, 27-36.
- Halverson, J. B., J. Simpson, G. Heymsfield, H. Pierce, T. Hock, and L. Ritchie, 2006: Warm core structure of Hurricane Erin diagnosed from high altitude dropsondes during CAMEX-4. *J Atmos Sci*, 63, 309-324.
- Hamill, T. M., and C. Snyder, 2000: A comparison of probabilistic forecasts from bred, singular vector, and perturbed observation ensembles. *Mon. Wea. Rev.*, 128, 1835-1851.
- Hawkins, H. F., and S. M. Imbembo, 1976: The structure of a small, intense hurricane-Inez 1966. *Mon. Wea. Rev.*, 104, 418-442.
- Hayden, C. M., and R. J. Purser, 1995: Recursive filter objective analysis of meteorological fields: applications to NESDIS operational processing. *J. Appl. Meteor.*, 34, 3-15.
- Hong, S.-Y., J. Dudhia, and S.-H. Chen, 2004: A revised approach to ice microphysical processes for the bulk parameterization of clouds and precipitation. *Mon. Wea. Rev.*, 132, 103-120.
- Houtekamer, P. L., L. Lefaivre, J. Derome, H. Ritchie, and H. L. Mitchell, 1996: A system simulation approach to ensemble prediction. *Mon. Wea. Rev.*, 124, 1225-1242.
- Hsiao, L. F., and Coauthors, 2010: A Vortex Relocation Scheme for Tropical Cyclone Initialization in Advanced Research WRF. *Mon Weather Rev*, 138, 3298-3315.
- Hu, M., M. Xue, J. Gao, and K. Brewster, 2006: 3DVAR and cloud analysis with WSR-88D level-II data for the prediction of Fort Worth tornadic thunderstorms. Part II: Impact of radial velocity analysis via 3DVAR. *Mon. Wea. Rev.*, 134, 699-721.
- Ito, K., M. Kunii, T. Kawabata, K. Saito, K. Aonashi, and L. Duc, 2016: Mesoscale Hybrid Data Assimilation System based on JMA Nonhydrostatic Model. *Mon Weather Rev*, 144, 3417-3439.
- Kain, J. S., 2004: The Kain-Fritsch convective parameterization: An update. *J Appl Meteorol*, 43, 170-181.
- Li, X., J. Ming, M. Xue, Y. Wang, and K. Zhao, 2015: Implementation of a dynamic equation constraint based on the steady state momentum equations within the WRF hybrid ensemble-3DVar data assimilation system and test with radar T-TREC wind assimilation for tropical Cyclone Chanthu (2010). *J Geophys Res-Atmos*, 120, 4017-4039.
- Li, Y., X. Wang, and M. Xue, 2012: Assimilation of radar radial velocity data with the WRF ensemble-3DVAR hybrid system for the prediction of hurricane Ike (2008). *Mon. Wea. Rev.*, 140, 3507-3524.

- Liu, Y., D.-L. Zhang, and M. K. Yau, 1999: A multiscale numerical study of hurricane Andrew (1992). Part II: Kinematics and inner-core structures. *Mon. Wea. Rev.*, 127, 2597-2616.
- Lorenc, A., 2003: The potential of the ensemble Kalman filter for NWP - a comparison with 4D-Var. *Quart. J. Roy. Meteor. Soc.*, 129, 3183-3204.
- Mlawer, E. J., S. J. Taubman, P. D. Brown, M. J. Iacono, and S. A. Clough, 1997: Radiative transfer for inhomogeneous atmospheres: RRTM, a validated correlated-k model for the longwave. *J. Geophys. Res.*, 102, 16663-16682.
- Noh, Y., W. G. Cheon, S. Y. Hong, and S. Raasch, 2003: Improvement of the K-profile model for the planetary boundary layer based on large eddy simulation data. *Boundary-Layer Meteorology*, 107, 401-427.
- Oye, R., M. C., and S. S., 1995: Software for radar translation, visualization, editing, and interpolation. Preprints, Preprints, 27th Conf. on Radar Meteorology, Vail, CO, 359-361.
- Parrish, D. F., and J. C. Derber, 1992: The National Meteorological Center's spectral statistical-interpolation analysis system. *Mon. Wea. Rev.*, 120, 1747-1763.
- Poterjoy, J., and F. Q. Zhang, 2014: Intercomparison and Coupling of Ensemble and Four-Dimensional Variational Data Assimilation Methods for the Analysis and Forecasting of Hurricane Karl (2010). *Mon Weather Rev*, 142, 3347-3364.
- Schaefer, J. T., 1990: The critical success index as an indicator of warning skill. *Wea. Forecasting*, 5, 570-575.
- Schenkman, A., M. Xue, A. Shapiro, K. Brewster, and J. Gao, 2011: The analysis and prediction of the 8-9 May 2007 Oklahoma tornadic mesoscale convective system by assimilating WSR-88D and CASA radar data using 3DVAR. *Mon. Wea. Rev.*, 139, 224-246.
- Shen, F. F., and J. Z. Min, 2015: Assimilating AMSU-A Radiance Data with the WRF Hybrid En3DVAR System for Track Predictions of Typhoon Megi (2010). *Adv Atmos Sci*, 32, 1231-1243.
- Shen, F. F., J. Z. Min, and D. M. Xu, 2016: Assimilation of radar radial velocity data with the WRF Hybrid ETKF-3DVAR system for the prediction of Hurricane Ike (2008). *Atmos Res*, 169, 127-138.
- Skamarock, W. C., J. B. Klemp, J. Dudhia, D. O. Gill, D. M. Barker, W. Wang, and J. D. Powers, 2005: A Description of the Advanced Research WRF Version 2. 32127, Number of 88pp.
- Song, J. J., Y. A. Wang, and L. G. Wu, 2010: Trend discrepancies among three best track data sets of western North Pacific tropical cyclones. *Journal of Geophysical Research-Atmospheres*, 115.
- Sugimoto, S., N. A. Crook, J. Sun, Q. Xiao, and D. Barker, 2009: Assimilation of Doppler radar data with WRF 3DVAR: Evaluation of its potential benefits to quantitative precipitation forecasting through observing system simulation experiments. *Mon. Wea. Rev.*, 137, 4011-4029.
- Sun, J. Z., and H. L. Wang, 2013: WRF-ARW Variational Storm-Scale Data Assimilation: Current Capabilities and Future Developments. *Adv Meteorol*.

- Torn, R. D., 2010: Performance of a Mesoscale Ensemble Kalman Filter (EnKF) during the NOAA High-Resolution Hurricane Test. *Mon Weather Rev*, 138, 4375-4392.
- Wang, M. J., M. Xue, and K. Zhao, 2016: The impact of T-TREC-retrieved wind and radial velocity data assimilation using EnKF and effects of assimilation window on the analysis and prediction of Typhoon Jangmi (2008). *J Geophys Res-Atmos*, 121, 259-277.
- Wang, M. J., M. Xue, K. Zhao, and J. L. Dong, 2014: Assimilation of T-TREC-Retrieved Winds from Single-Doppler Radar with an Ensemble Kalman Filter for the Forecast of Typhoon Jangmi (2008). *Monthly Weather Review*, 142, 1892-1907.
- Wang, X., 2011: Application of the WRF hybrid ETKF-3DVAR data assimilation system for hurricane track forecasts. *Wea. and Forecasting*, 26.
- Wang, Y. B., J. Z. Min, Y. D. Chen, X. Y. Huang, M. J. Zeng, and X. Li, 2017: Improving precipitation forecast with hybrid 3DVar and time-lagged ensembles in a heavy rainfall event. *Atmos Res*, 183, 1-16.
- Wu, C. C., G. Y. Lien, J. H. Chen, and F. Q. Zhang, 2010: Assimilation of Tropical Cyclone Track and Structure Based on the Ensemble Kalman Filter (EnKF). *J Atmos Sci*, 67, 3806-3822.
- Xiao, Q., and J. Sun, 2007: Multiple radar data assimilation and short-range quantitative precipitation forecasting of a squall line observed during IHOP_2002. *Mon.Wea.Rev.*, 135, 3381-3404.
- Xie, Y. F., and A. E. MacDonald, 2012: Selection of Momentum Variables for a Three-Dimensional Variational Analysis. *Pure and Applied Geophysics*, 169, 335-351.
- Yu, H., C. Hu, and L. Jiang, 2007: Comparison of three tropical cyclone intensity datasets. *Acta Meteorologica Sinica.*, 21, 121 - 128.
- Zhang, F., Y. Weng, J. A. Sippel, Z. Meng, and C. H. Bishop, 2009: Cloud-resolving hurricane initialization and prediction through assimilation of Doppler radar observations with an ensemble Kalman filter. *Mon. Wea. Rev.*, 137, 2105-2125.
- Zhao, K., W. C. Lee, and B. J. D. Jou, 2008: Single Doppler radar observation of the concentric eyewall in Typhoon Saomai, 2006, near landfall. *Geophys. Res. Lett.*, 35, L07807.
- Zhao, K., M. Xue, and W. C. Lee, 2012: Assimilation of GBVTD-retrieved winds from single-Doppler radar for short-term forecasting of super typhoon Saomai (0608) at landfall. *Quarterly Journal of the Royal Meteorological Society*, 138, 1055-1071.
- Zhu, L., and Coauthors, 2016: Prediction and Predictability of High-Impact Western Pacific Landfalling Tropical Cyclone Vicente (2012) through Convection-Permitting Ensemble Assimilation of Doppler Radar Velocity. *Mon Weather Rev*, 144, 21-43.

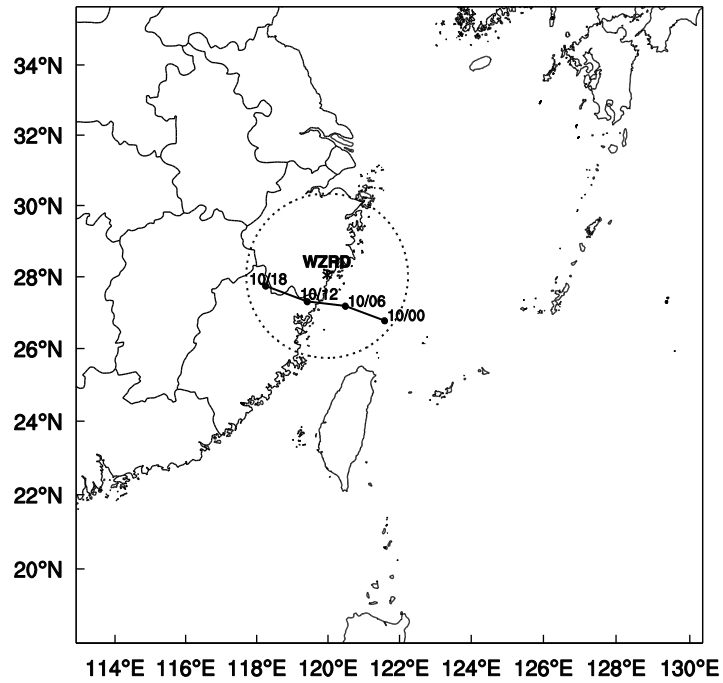


Figure1. The WRF model domain and best track positions for typhoon Saomai (2006) from CMA from 0000 UTC 10 to 1800 UTC 10 August 2006. Also indicated are the WZRD location and maximum range coverage circles.

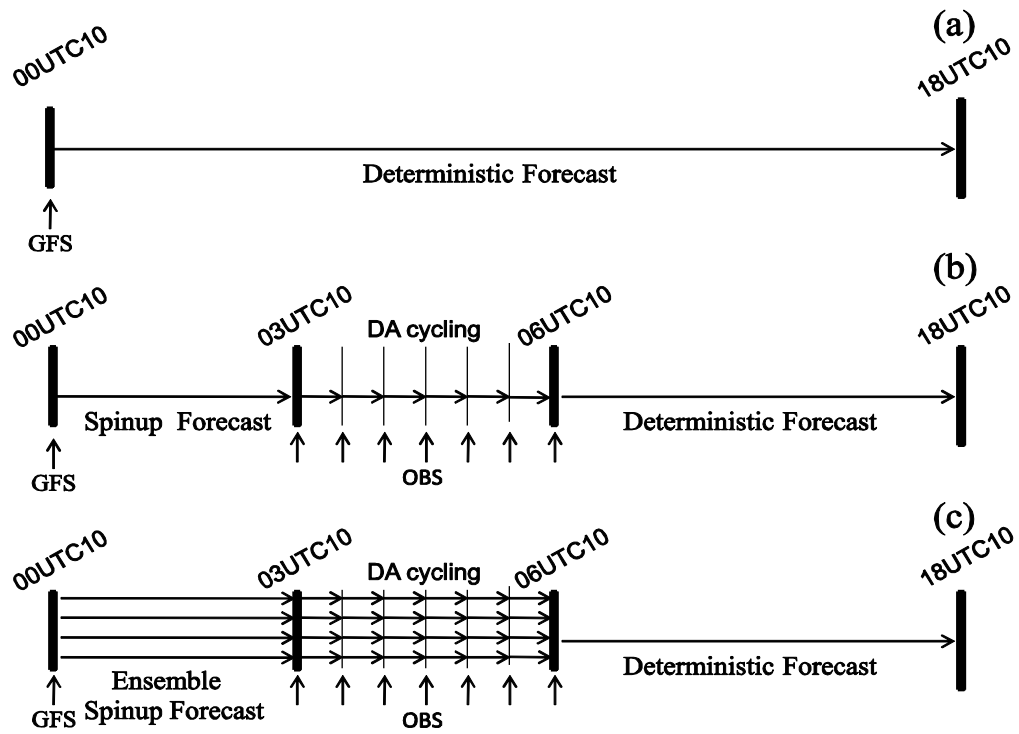


Figure 2. The flow charts for (a) NoDA experiment, (b) 3DVAR experiments (3DVARa and 3DVARb), and (c) hybrid experiments (HybridF and HybridH) initialized at 00UTC 10 August 2006.

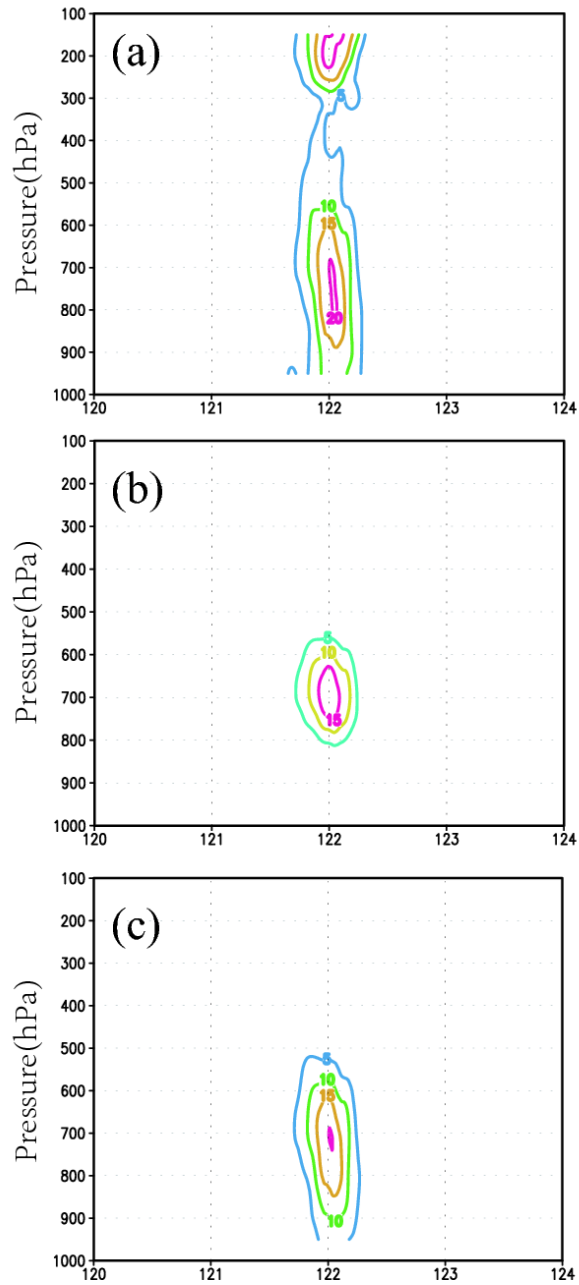


Figure3. The vertical cross section of the wind speed increment using a single WZRD Vr data point located at (26.919°N, 121.983°E; 3306.7m) using the configurations of experiment HybridF for (a) vertloc_no, (b) vertloc_d, and (c) vertloc_km at 0300 UTC 10 Aug 2006.

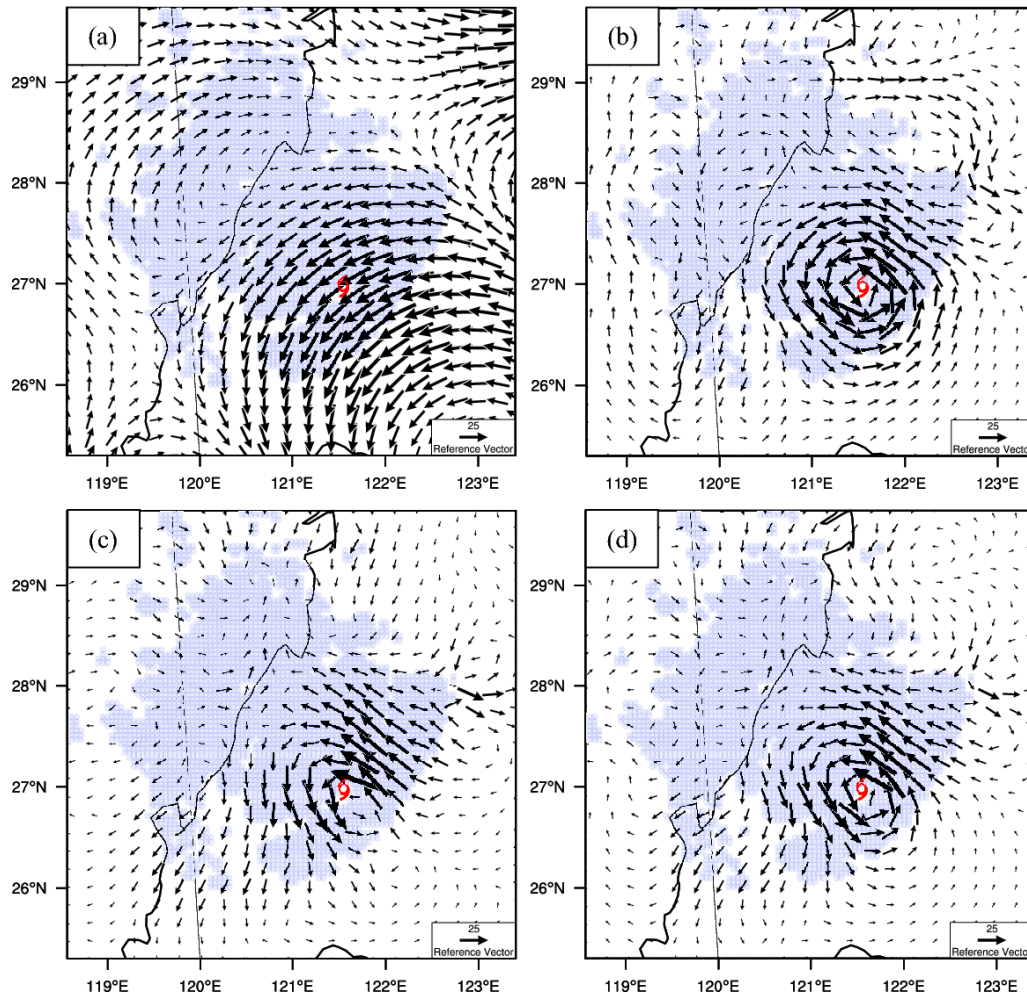


Figure 4. The 700 hPa wind analysis increments (m s^{-1}) for (a) 3DVARa, (b) 3DVARb, (c) HybridF, and (d) HybridH at 0300 UTC 10 August 2006. The red typhoon symbol is the typhoon center from best track.

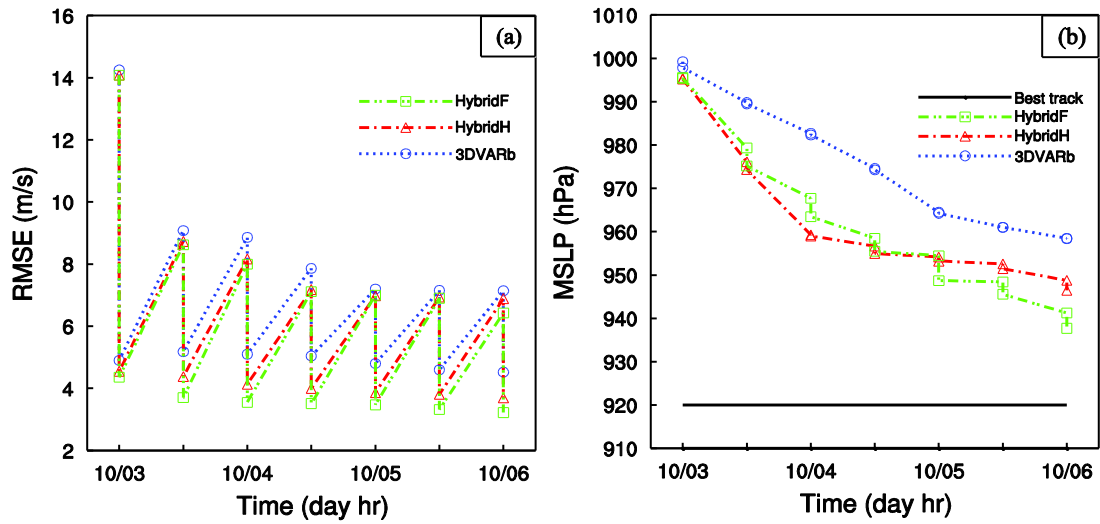


Figure 5. The forecast and analysis (sawtooth pattern during DA cycling) of (a) RMSE of radial velocity (m s^{-1}), and (b) the minimum sea level pressures (hPa) together with the CMA best track estimate, for 3DVARb, HybridF, and HybridH from 0300 to 0600 UTC 10 August 2006.

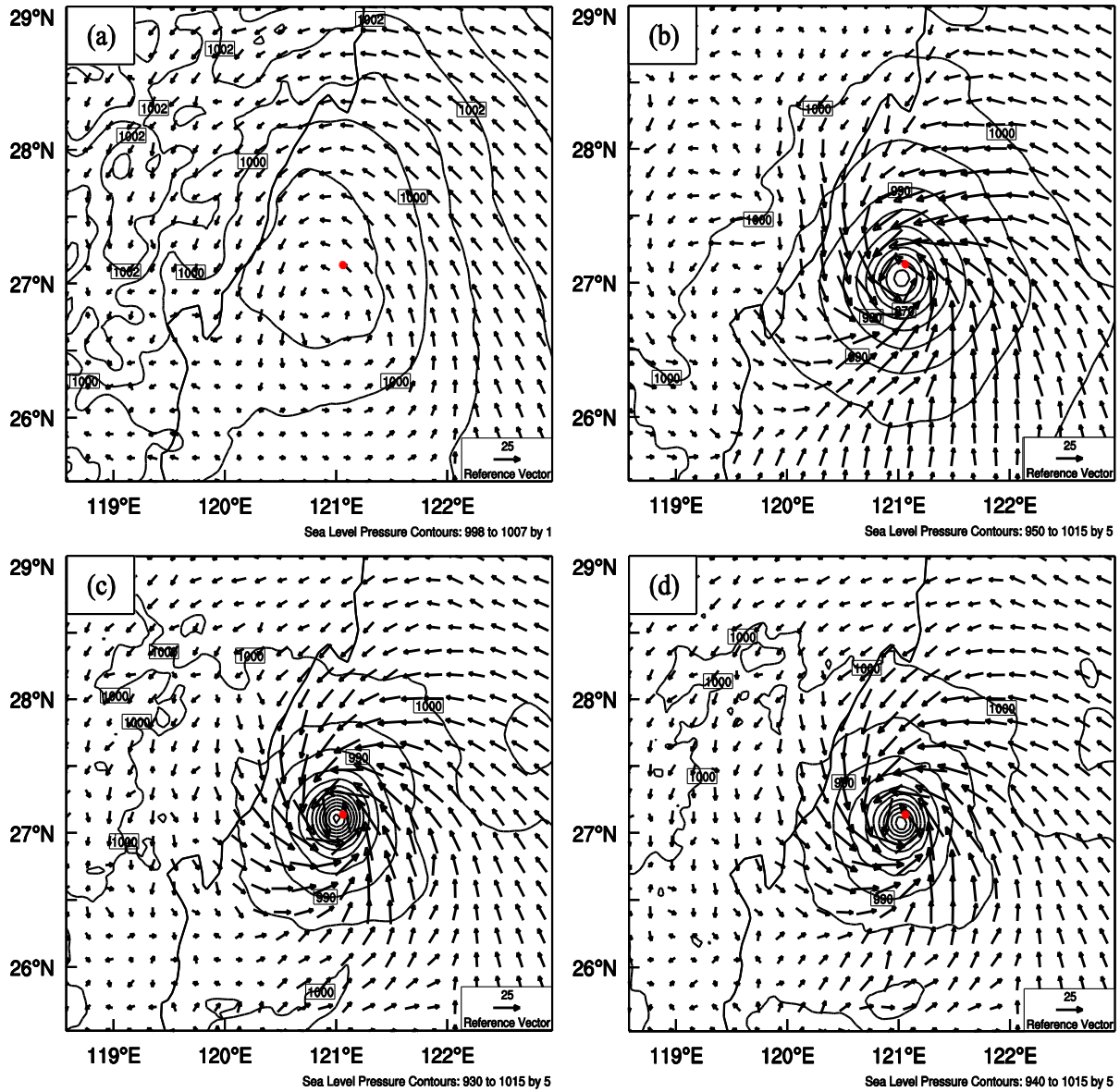


Figure 6. The analyzed sea level pressure (solid contours) and the surface wind vectors (m s^{-1}) for (a) NoDA, (b) 3DVARb, (c) HybridF, and (d) HybridH at 0600 UTC 10 August 2006. The red dot in the panels are observed typhoon center.

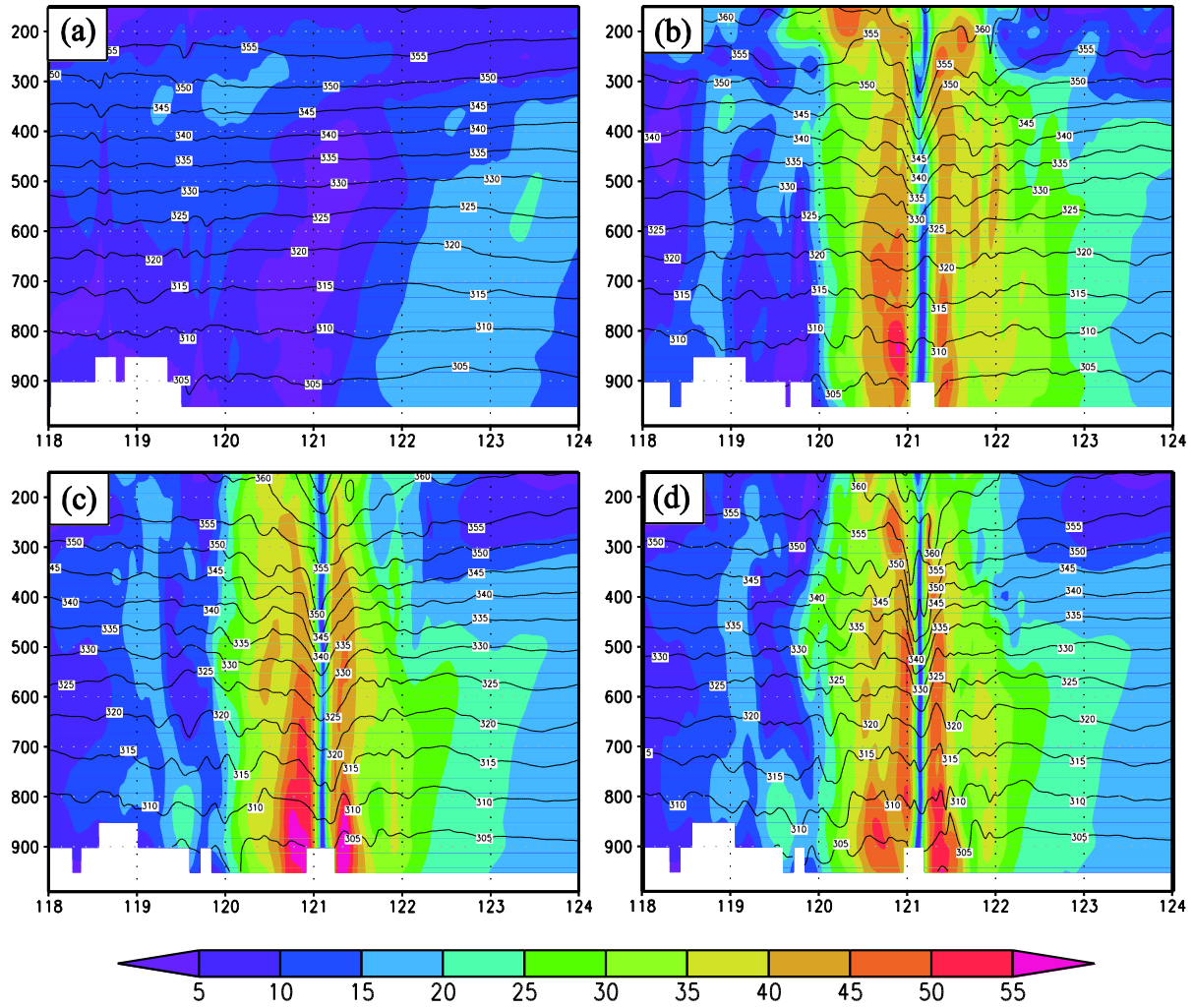


Figure 7. Vertical cross sections of analyzed horizontal wind speed (interval of 5 m s^{-1} , shaded) and potential temperature (interval of 5 K , solid contours) for (a) NoDA, (b) 3DVARb, (c) HybridF, and (d) HybridH, at 0600 UTC 10 August 2006.

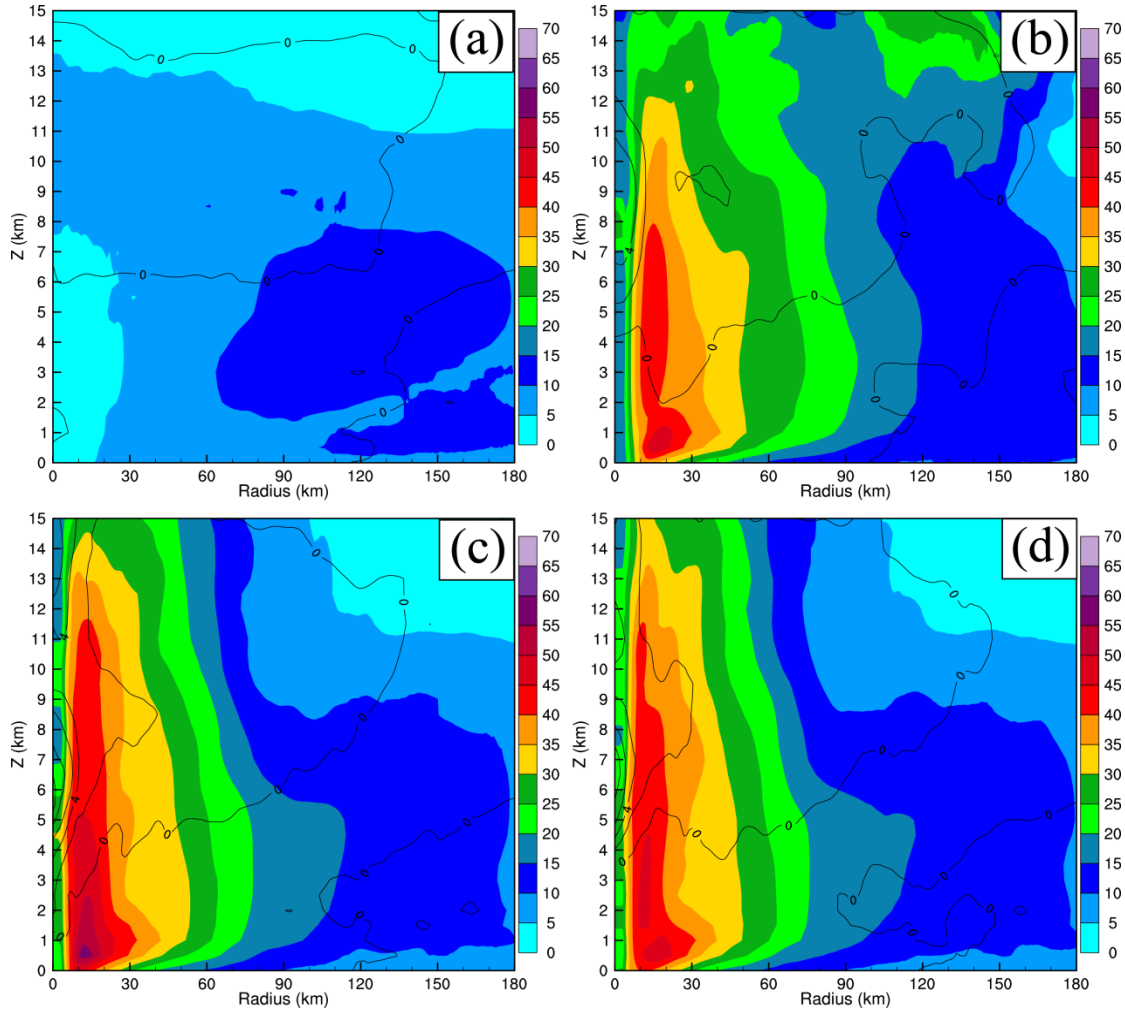


Figure 8. Radius-height plots of azimuthally averaged tangential wind (color shaded contours, m s⁻¹) and temperature anomaly (solid contours with intervals of 2 K) at 0600 UTC for experiments (a) NoDA, (b) 3DVARb, (c) HybridF, and (d) HybridH.

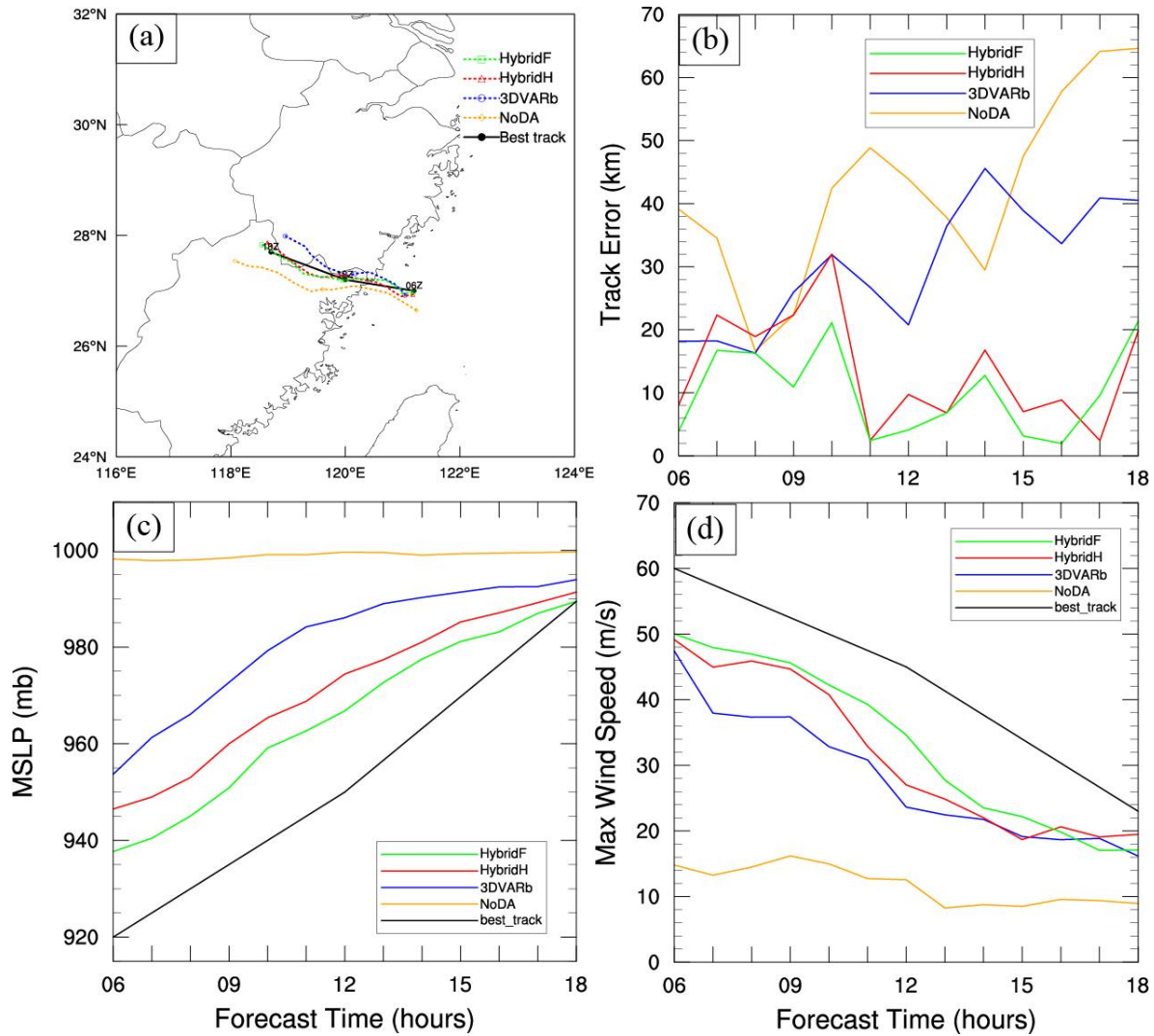


Figure 9. The predicted (a) tracks, (b) track errors, (c) minimum SLP, and (d) maximum surface winds speed by NoDA, 3DVARb, HybridF, and HybridH as compared to CMA best track estimates from 0600 UTC to 1800 UTC 10 August 2006.

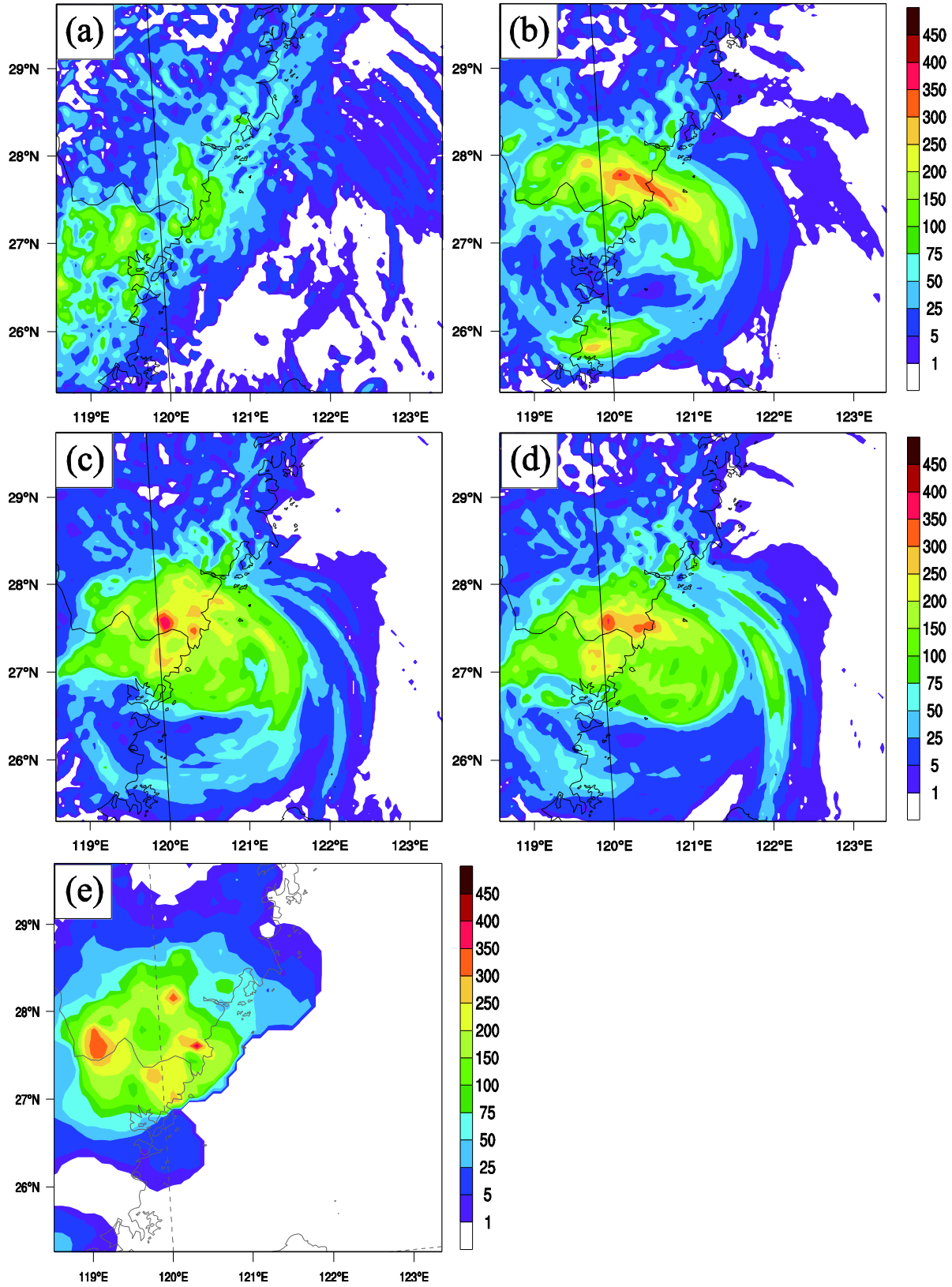


Figure 10. 12h accumulated precipitation from 0600 UTC to 1800 UTC 10 August for (a) NoDA, (b) 3DVARb, (c) HybridF, (d) HybridH, and (e) automatic weather station observations.

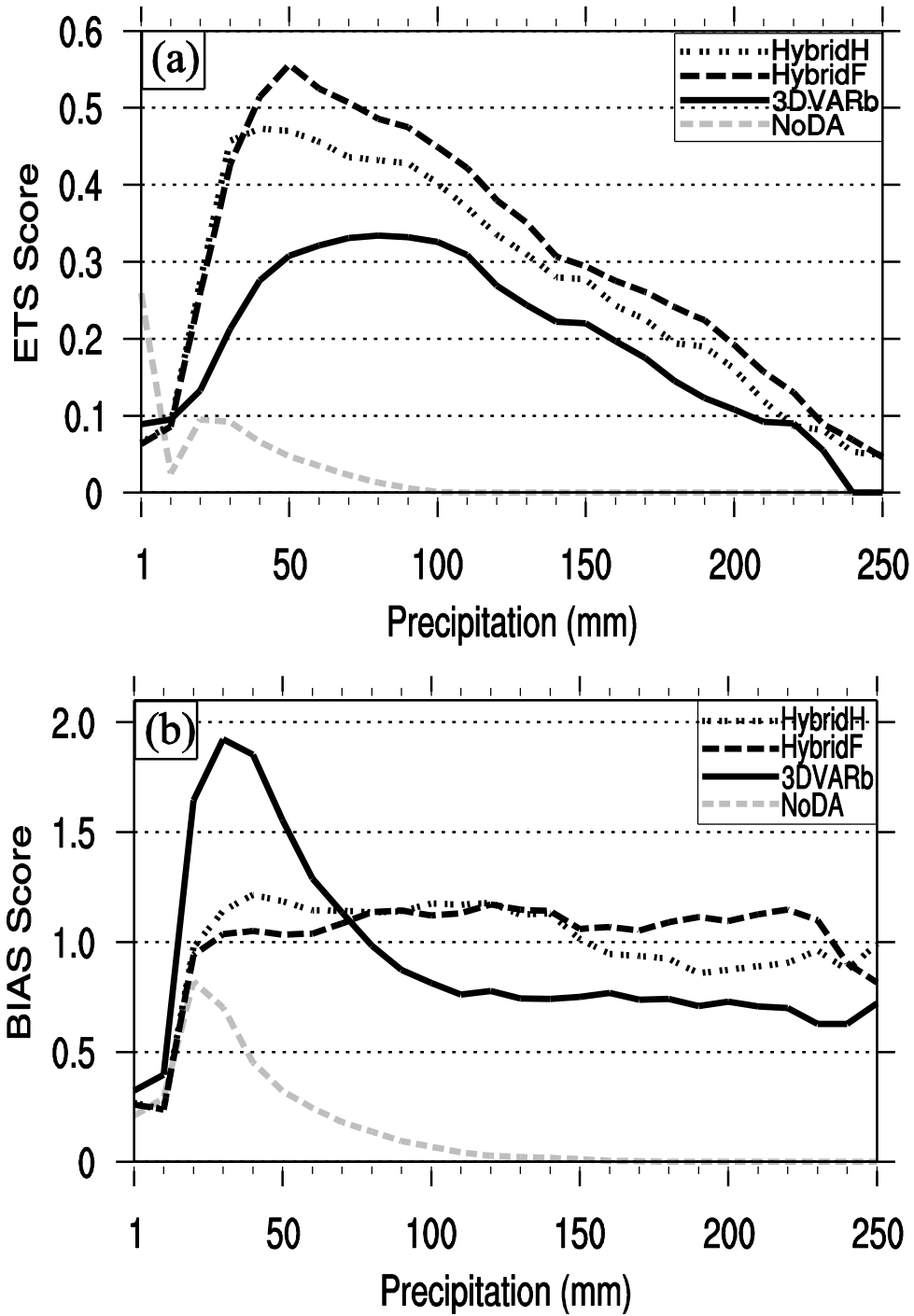


Figure 11. (a) Equitable threat scores and (b) biases of the 12h accumulated precipitation verified against automatic weather station observations for NoDA, 3DVARb, HybridF, and HybridH.

Table 1. List of experiments

Experiment	Description
NoDA	No radar data assimilation. WRF model initial condition interpolated

	from NCEP 1°x1° analysis
3DVARa	Radar DA using WRF 3DVAR with static covariance from NMC method
3DVARb	Same as 3DVARa, except the horizontal spatial correlation in the static covariance is multiplied by 0.1.
HybridF	Radar DA using hybrid method with full weight given to flow dependent covariance, with $1/b_1 = 1/1001$ and $1/b_2 = 1/1.001$ in Eq. (1)
HybridH	Hybrid method with equal weight given to static covariance (which is the same as 3DVARb) and flow-dependent covariance, with $1/b_1 = 1/2$ and $1/b_2 = 1/2$ in Eq. (1)
